Received: 2 May 2022 | Revised: 27 July 2022 | Accepted: 12 August 2022

IET Communications

DOI: 10.1049/cmu2.12489

The Institution of Engineering and Technology WILEY

ORIGINAL RESEARCH

Performance analysis of communications systems with radar interference and hardware impairment

Junqiu Wang | **Yunfei Chen**

The School of Engineering, University of Warwick, Coventry, UK

Correspondence
Junqiu Wang, School of Engineering, University of Warwick, Coventry CV4 7AL, UK.
Email: Qiuqiu.Wang@warwick.ac.uk

Abstract

The development of future wireless communications systems faces a big challenge of spectrum scarcity. Co-existence of radar and communications systems is thus of great interest. In this work, the performance of a communications system with hardware impairment (HWI) as well as interference from radar systems will be studied. The impact of radar interference, I/Q imbalance coefficients as well as channel state information (CSI) will be evaluated in terms of outage probability and symbol error rate. Simulation results prove that the proposed detectors provide explicit and conducive insights for further exploration of joint radar-communications designs.

1 | INTRODUCTION

Wireless communications systems are undergoing dramatic changes. This makes the radio spectrum scarce. To alleviate this problem, the coexistence of radar and communications systems was proposed [1]. The core challenge in their coexistence is their mutual interference [2]. Several works have studied the interference between radar and communications. Some focused on the performance of radar system in the presence of communications interference. In [3], the bounds of target detection and missing probability were derived under cellular interference. In [4], radar waveform design was studied to maintain the detection performance while not compromising the symbol error rate of the communications system. The adaptive placement of radar receivers to collectively mitigate interference from communications systems was also studied in [5]. Others investigated the performance of communications systems when radar interference is present due to spectrum sharing. For example, reference [6] extended channel sensing to develop a packet scheduling algorithm that slightly degraded the long-term evolution (LTE) system's performance. The impact of directly injected narrowband radar interference on the LTE down-link was investigated in [7]. A method to mitigate this interference and improve LTE throughput was proposed. The authors in [8] studied constellation design for the communications systems with radar interference and expanded the design to multi-carrier orthogonal frequency division multiplexing (OFDM). The aforementioned works are all based on interference cancellation (IC). However, IC will not always be effective in future ulta-densely connected and mobile networks [9]. Thus, a new kind of scheme to achieve coexistence between communications and radar is dual functional radar-communication (DFRC), where the key point is to integrate radar and communication waveforms into a single transmitted signal so that this signal is capable of simultaneous communication and sensing [10]. One design of DFRC is the radar/communications-centric scheme that is typically designed to realize one system function without significantly compromising the performance of the other. In [11], data embedding method and a novel symbol mapping constellation scheme were proposed to improve the spectrum efficiency in the monostatic broadcast topology. In [12], a zero-forcing beamforming design was proposed to solve the weighted radar performance sum problem while guaranteeing the minimum communications performance. The integration of communications and full duplex radar was investigated for vehicle-to-vehicle (V2V) scenario in [13] and for the fourth-generation LTE and fifth-generation (5G) new radio (NR) scenarios in [14]. Another design of DFRC is to fulfill various desired application scenarios without prioritizing either sensing or communications. The authors focused on waveform multiplexing designs and proposed low-complexity super-resolution algorithms for joint bi-static automotive radar and vehicle-to-vehicle communications using millimeter-wave in [15]. A penalized weighted sum problem was introduced and solved by efficient manifold algorithms in [16].

All these studies have shed lights on the interference between radar and communication systems but they have ignored the hardware impairment (HWI) by assuming perfect equipment. However, recent studies have pointed out that the communication system performance is largely affected by HWI so that HWI cannot be ignored, since these hardware imperfections will cause phase and amplitude mismatch, raise noise floor or distort image signals [17]. For example, [18] pointed out that HWI could make a huge difference when planning and deploying the next-generation joint radar-communication systems. There are different types of HWI: phase noise [19], high power amplifier nonlinearity [20], in-phase/quadrature-phase imbalance (IQI) [21], and frequency/phase offset [22] etc. Several works have studied the performances of wireless systems, including ergodic capacity, symbol error rate and outage probability, with HWI. For example, in [23], the authors investigated the direct-conversion radio (DCR) receivers' energy detection performance with radio frequency (RF) impairment. Reference [24] considered residual HWI in a non-orthogonal multiple access (NOMA) system. Reference [25] studied the amplify-and-forward (AF) and decode-and-forward (DF) relaying performances with hardware impairment. The above discussion shows that HWI is important and indispensable to improve the performance of future radar-communications coexistence designs. However, to the best of our knowledge, none of existing works on coexistence of radar and communications systems has considered HWI. This motivates us to fill this gap. For unaltered legacy radars where reinstalling the hardware is too costly, it is relevant to delve into more reliable radar-communications coexistence frameworks that do not compromise the performance of the communications system. In this work, a system model for the integrated signal as the input of the communications receiver in presence of HWI is established. Our purpose is to understand the combined impact of radar interference, HWI and CSI. Similar to [26–28], we focus on IQI which is one of the most common HWI types. For the radio frequency (RF) front-end in a communications system, it is critical to process the signals in the passband at both transmitter and receiver. This requires the in-phase (I) and quadrature (Q) branches. For the two main RF fronts, direct-conversion (also referred as zero-intermediate frequency (IF) or homodyne) and superheterodyne, both suffer from the severe I/Q mismatch when the orthogonality between I and Q branches are destroyed to degrade the signal quality. This leads to the I/Q imbalance (IQI). Our study has the following contributions:

1) The analytical expression of the outage probability in the presence of radar interference and HWI is derived.
2) Novel coherent and noncoherent detectors are proposed taking into account HWI, which demonstrates that the consideration of HWI significantly improves the overall system performance.
3) The superiority of the coherent detector in terms of symbol error rate is proven by comparing it with the proposed noncoherent detector and the conventional detector as a benchmark under different scenarios. The impact of radar interference, IQI coefficients and CSI is rigorously investigated to provide choice of different detectors in different situations.
4) The symbol error rate for the proposed coherent detector is derived analytically, and is verified by simulation.

TABLE 1 Relevant symbol notations

Notation	Definition
G_1, G_2	IQI coefficients at the transmitter
K_1, K_2	IQI coefficients at the receiver
a_t	Amplitude mismatch of the transmitter
a_r	Amplitude mismatch of the receiver
ϕ_t	Phase mismatch of the transmitter
ϕ_r	Phase mismatch of the receiver
h	Channel coefficient
P_s	Signal transmission power
X	Desired complex baseband signal
$\sqrt{I}$	Radar interference amplitude
θ	Radar interference phase
Z	Additive white Gaussian noise (AWGN)
σ_X^2	Average signal power
$\tilde{\sigma}_x^2$	Signal pseudo variance
σ_h^2	Channel gain variance
σ_Z^2	AWGN variance
σ_e^2	CSI error variance
Y	The final received signal
S	Signal part of Y
W	Interference part of Y
N	Noise part of Y
r	Threshold for outage

2 | SYSTEM MODEL

In a practical communications system, it is very difficult to achieve perfect matching between the I and Q branches at TX/RX, since there is inevitable inaccuracy in the RF front-end implementation [21]. Consider a wireless communications system whose transmitter and receiver suffer from IQI. A list of relevant symbol notations are given by Table 1.

Denote $\omega_c = 2\pi f_c$ where f_c is the carrier frequency. The desired complex baseband signal X up-converted for transmission has an average signal power $\mathrm{E}(|X|^2) = \sigma_X^2$. Thus. the passband signal to be transmitted is

$$X_{RF} = \mathrm{Re}\left\{Xe^{j\omega_c t}\right\}, \tag{1}$$

where Re{·} gives the real part of its argument. Due to the IQI, there exists phase and amplitude mismatches caused by the local oscillator (LO) and power amplifier. Therefore, the distorted RF

signal is

$$X'_{\mathrm{RF}} = \mathrm{Re}\left\{ \left(\frac{1 + a_t e^{j\phi_t}}{2} X + \frac{1 - a_t e^{j\phi_t}}{2} X^*\right) e^{j\omega_c t} \right\}, \tag{2}$$

where a_t and ϕ_t are the amplitude and phase mismatches at the transmitter, respectively [21]. Denote $G_1 = \frac{1+a_t e^{j\phi_t}}{2}$ and $G_2 = 1 - {G_1}^*$, then the baseband signal after distortion by IQI at the transmitter becomes

$$Y_1 = G_1 X + G_2^* X^*. \tag{3}$$

The signal Y_1 is then transmitted with a transmission power of P_s through the fading channel with channel coefficient $h \sim CN(0, \sigma_h^2)$. In addition to the additive white Gaussian noise (AWGN) with $Z \sim CN(0, \sigma_Z^2)$, there is also additive radar interference in the channel. Using the radar interference model in [29], the amplitude of radar interference can be approximately as a constant, as its periodical pulses have very large amplitude and very short duration. The radar interference amplitude $\sqrt{I}$ is either known to the communications system or can be estimated at the receiver. Therefore, the additive radar interference is assumed to have a deterministic and constant amplitude. However, the radar interference phase θ varies rapidly because of multipath propagation so that it is modelled as uniformly distributed on $[0, 2\pi]$ [29]. The received signal is

$$Y_2 = \sqrt{P_s} h Y_1 + \sqrt{I} e^{j\theta} + Z. \tag{4}$$

Similarly, the signal in (4) suffers from IQI at the receiver to give

$$Y = K_1 Y_2 + K_2 Y_2^*, \tag{5}$$

where $K_1 = \frac{1+a_r e^{-j\phi_r}}{2}$, $K_2 = 1 - {K_1}^*$, a_r and ϕ_r are the amplitude and phase mismatches at the receiver due to the IQI, respectively. In our work, we assume that a_t, a_r, ϕ_t and ϕ_r are all fixed and known to the communications system.

3 | OPTIMAL DETECTOR

3.1 | Coherent detector

From (5), one has

$$Y = S + W + N, \tag{6}$$

where the signal, interference and noise parts are, respectively

$$S = \sqrt{P_s}[(K_1 h G_1 + K_2 h^* G_2) X + (K_1 h G_2^* + K_2 h^* G_1^*) X^*], \tag{7}$$

$$W = \sqrt{I}\left(K_1 e^{j\theta} + K_2 e^{-j\theta}\right), \tag{8}$$

$$N = K_1 Z + K_2 Z^*. \tag{9}$$

The introduction of the IQI at the receiver makes N an improper Gaussian variable [30]. Therefore, Y is also improper Gaussian. For further discussion, denote the real and imaginary parts of Z as Z_R and Z_I, respectively, with $Z = Z_R + Z_I i$. Since $Z \sim CN(0, \sigma_Z^2)$, one has

$$\begin{cases} \mathrm{E}(Z_R) = \mathrm{E}(Z_I) = 0 \\ \mathrm{E}(|Z|^2) = \mathrm{E}(Z_R^2) + \mathrm{E}(Z_I^2) = \sigma_Z^2 \\ \mathrm{E}(Z^2) = \mathrm{E}(Z_R^2) - \mathrm{E}(Z_I^2) + 2\,\mathrm{E}(Z_R Z_I) i = 0. \end{cases} \tag{10}$$

From (10), one has $\mathrm{E}(Z_R^2) = \mathrm{E}(Z_I^2) = \frac{\sigma_Z^2}{2}$.

Then, (9) is expanded as

$$N = Z_R + \left[(a_r \cos\phi_r) Z_I - (a_r \sin\phi_r) Z_R\right] i. \tag{11}$$

Denote N_R and N_I as the real and imaginary parts of N, respectively. Then, one has

$$\begin{cases} N_R = Z_R \\ N_I = \left[(a_r \cos\phi_r) Z_I - (a_r \sin\phi_r) Z_R\right]. \end{cases} \tag{12}$$

Since $\mathrm{E}(Z_R) = \mathrm{E}(Z_I) = 0$ and Z_R is independent of Z_I, one has

$$\begin{cases} \sigma_{N_R}^2 = \dfrac{\sigma_Z^2}{2} \\ \sigma_{N_I}^2 = a_r^2 \dfrac{\sigma_Z^2}{2} \\ \mathrm{E}(N_R N_I) = -(a_r \sin\phi_r) \dfrac{\sigma_Z^2}{2}. \end{cases} \tag{13}$$

The correlation coefficient between N_R and N_I is

$$\rho = \frac{\mathrm{E}(N_R N_I)}{\sigma_{N_R} \sigma_{N_I}} = -\sin\phi_r. \tag{14}$$

According to [30], we have the joint probability density function (PDF) $f(y_R, y_I)$ as

$$\frac{e^{-\frac{\frac{[y_R - (S_R + W_R)]^2}{\sigma_{N_R}^2} + \frac{[y_I - (S_I + W_I)]^2}{\sigma_{N_I}^2} - \frac{2\rho[y_R - (S_R + W_R)][y_I - (S_I + W_I)]}{\sigma_{N_R}\sigma_{N_I}}}{2(1-\rho^2)}}}{2\pi\sqrt{1-\rho^2}\,\sigma_{N_R}\sigma_{N_I}}. \tag{15}$$

By putting (13) and (14) into (15), the joint PDF can be further simplified as

$$f(y_R, y_I) = \frac{1}{\pi (a_r |\cos\phi_r|) \sigma_Z^2} e^{-\frac{a_r^2 A^2 + B^2 + 2(a_r \sin\phi_r) AB}{(a_r \cos\phi_r)^2 \sigma_Z^2}} \tag{16}$$

where $A = y_R - (S_R + W_R)$ and $B = y_I - (S_I + W_I)$, y_R, S_R and W_R are the real parts of y, S and W, respectively, y_I, S_I and W_I are the imaginary parts of y, S and W, respectively, and all other

symbols are defined as before. The detection is to choose the transmitted signal X that maximizes (16), or

$$\hat{X} = \min_X \left\{ a_r^2 A^2 + B^2 + 2(a_r \sin\phi_r)AB \right\}. \tag{17}$$

We further note that

$$\int_0^{2\pi} \frac{1}{2\pi} e^{\frac{2\sqrt{I}k_1}{\sigma_Z^2}\cos\left(\theta+\theta'\right)} d\theta = \frac{1}{2\pi}\cdot 2\cdot \int_0^{\pi} e^{\frac{2\sqrt{I}k_1\cos\theta}{\sigma_Z^2}} d\theta = \frac{1}{\pi}\int_0^{\pi} e^{\frac{2\sqrt{I}k_1\cos\theta}{\sigma_Z^2}} d\theta. \tag{24}$$

$$f(y_R, y_I|\theta) = \frac{e^{-\left[\underbrace{(-2(a_r\sin\phi_r)A_1 - 2B_1)W_I}_{①} + \underbrace{(-2(a_r\sin\phi_r)B_1 - 2A_1a_r^2)W_R}_{②}\right]/(a_r\cos\phi_r)^2\sigma_Z^2 + \left[\underbrace{(a_r^2W_R^2 + W_I^2 + 2(a_r\sin\phi_r)W_RW_I)}_{③} + \underbrace{(a_r^2A_1^2 + B_1^2 + 2(a_r\sin\phi_r)A_1B_1)}_{④}\right]/(a_r\cos\phi_r)^2\sigma_Z^2}}{\pi(a_r|\cos\phi_r|)\sigma_Z^2}. \tag{18}$$

$$① = (-2(a_r\sin\phi_r)A_1 - 2B_1)\sqrt{I}(a_r\cos\phi_r\sin\theta - a_r\sin\phi_r\cos\theta)$$
$$= 2\sqrt{I}a_r\left(-(a_r\sin\phi_r\cos\phi_r)A_1\sin\theta - (\cos\phi_r)B_1\sin\theta + (a_r\sin^2\phi_r)A_1\cos\theta + (\sin\phi_r)B_1\cos\theta\right) \tag{19}$$

$$② = 2\sqrt{I}a_r(-(\sin\phi_r)B_1\cos\theta - a_rA_1\cos\theta) \tag{20}$$

$$③ = Ia_r^2(\cos^2\theta + \cos^2\phi_r\sin^2\theta - \sin^2\phi_r\cos^2\theta) = Ia_r^2\cos^2\phi_r \tag{21}$$

Note that y_R is related to A and y_I is related to B in (17).

3.2 | Noncoherent detector

The density function in (15) contains the known information of θ while it is unknown for the noncoherent detection. By denoting $A_1 = y_R - S_R$ and $B_1 = y_I - S_I$ and keeping all other symbols the same as those in (16), (15) can be expressed as (18) at the top of this page which depends on θ. Using (19)-(21), one could rewrite (18) as

$$f(y_R, y_I|\theta) = \frac{e^{-\frac{k_1^2+I}{\sigma_Z^2}}}{\pi(a_r|\cos\phi_r|)\sigma_Z^2} e^{\frac{2\sqrt{I}k_1\cos\left(\theta+\theta'\right)}{\sigma_Z^2}}, \tag{22}$$

where $\theta' = -\arctan\frac{B_1+(a_r\sin\phi_r)A_1}{(a_r\cos\phi_r)A_1}$, $k_1 = \frac{\sqrt{a_r^2A_1^2+B_1^2+2(a_r\sin\phi_r)A_1B_1}}{a_r|\cos\phi_r|}$. The unconditional function is calculated as

$$f(y_R, y_I) = \frac{e^{-\frac{k_1^2+I}{\sigma_Z^2}}}{\pi(a_r|\cos\phi_r|)\sigma_Z^2}\int_0^{2\pi}\frac{1}{2\pi}e^{\frac{2\sqrt{I}k_1}{\sigma_Z^2}\cos\left(\theta+\theta'\right)}d\theta. \tag{23}$$

Therefore, (23) becomes

$$f(y_R, y_I) = \frac{e^{-\frac{k_1^2+I}{\sigma_Z^2}}}{\pi(a_r|\cos\phi_r|)\sigma_Z^2} I_0\left(\frac{2\sqrt{I}k_1}{\sigma_Z^2}\right), \tag{25}$$

where $I_0(x)$ is the zero'th order modified Bessel function of the first type. Similar to (17), the new noncoherent detector considering both radar interference and HWI is

$$\hat{X}_1 = \min_X \left\{ \frac{k_1^2}{\sigma_Z^2} - \ln\left(I_0\left(\frac{2\sqrt{I}k_1}{\sigma_Z^2}\right)\right)\right\}. \tag{26}$$

For comparison, the noncoherent detector in [8] without considering HWI is given as

$$\hat{X}_2 = \arg\min_X \left\{ \left|y - \sqrt{S}X\right|^2 - \ln I_0\left(2\sqrt{I}\left|y - \sqrt{S}X\right|\right)\right\}. \tag{27}$$

4 | PERFORMANCE ANALYSIS

4.1 | Outage probability

The power of S is $|S|^2 = SS^*$. From (7), $|S|^2$ is further calculated as

$$P_s\left(\left|(K_1hG_1 + K_2h^*G_2)X\right|^2 + \left|\left(K_1hG_2^* + K_2h^*G_1^*\right)X^*\right|^2\right) + 2P_s\left(Re((K_1hG_1 + K_2h^*G_2)X\left(\left(K_1hG_2^* + K_2h^*G_1^*\right)X^*\right)^*)\right)$$
$$= P_s\left(|K_1hG_1 + K_2h^*G_2|^2|X|^2 + |K_1hG_2^* + K_2h^*G_1^*|^2|X|^2\right) + 2P_s\left(Re((K_1hG_1 + K_2h^*G_2)\left(K_1hG_2^* + K_2h^*G_1^*\right)^*X^2)\right). \tag{28}$$

Since $\mathrm{E}(X^2) = \widetilde{\sigma_X}^2$, $\mathrm{E}(|X|^2) = \sigma_X^2$, by expanding (28), one has

$$\begin{aligned}\mathrm{E}\left(|S|^2\right) &= P_s|h|^2\left(|K_1|^2 + |K_2|^2\right)\\ &\times\left[|G_1|^2\sigma_X^2 + |G_2|^2\sigma_X^2 + 2\,\mathrm{Re}\left(G_1G_2\widetilde{\sigma_X^2}\right)\right]\\ &+ 2P_s\mathrm{Re}\left[K_1K_2^*h^2\left(2G_1G_2^*\sigma_X^2 + G_1^2\widetilde{\sigma}_X^2 + (G_2^*)^2\widetilde{\sigma_X^2}^*\right)\right].\end{aligned} \tag{29}$$

For W and N, from (8) and (9) one can similarly derive that

$$\mathrm{E}\left(|W+N|^2\right) = \left(|K_1|^2 + |K_2|^2\right)\left(I + \sigma_Z^2\right) + 2I\,\mathrm{Re}(K_1K_2^*e^{j2\theta}). \tag{30}$$

The outage probability is calculated as

$$P_o = \int_0^{2\pi}\frac{1}{2\pi}Pr\left(\frac{\mathrm{E}(|S|^2)}{\mathrm{E}(|W+N|^2)} < r|\theta\right)d\theta \tag{31}$$

where r is the outage threshold. It is predetermined based on the communications performance requirements. For $\frac{\mathrm{E}(|S|^2)}{\mathrm{E}(|W+N|^2)} < r$, it can be transformed into

$$\begin{aligned}&\left(C + 2\,\mathrm{Re}(D)\right)h_R^2 - 4\,\mathrm{Im}(D)h_Rh_I + \left(C - 2\,\mathrm{Re}(D)\right)h_I^2\\ &< \frac{r\left(|K_1|^2 + |K_2|^2\right)\left(I + \sigma_Z{}^2 + 2I\,\mathrm{Re}(K_1K_2^*e^{j2\theta})\right)}{P_s},\end{aligned} \tag{32}$$

where

$$\begin{aligned}C = &\left(|K_1|^2 + |K_2|^2\right)\cdot\\ &\left[|G_1|^2\sigma_X^2 + |G_2|^2\sigma_X^2 + 2\,\mathrm{Re}\left(G_1G_2\widetilde{\sigma_X^2}^*\right)\right],\end{aligned} \tag{33}$$

$D = K_1K_2^*(2G_1G_2^*\sigma_X^2 + G_1^2\widetilde{\sigma}_X^2 + (G_2^*)^2\widetilde{\sigma_X^2}^*)$, h_R and h_I are the real and imaginary parts of h, respectively. Since $h \sim CN(0, \sigma_h^2)$, (32) is regarded as the inequality of a quadratic form of two independent normal random variables. With this, (32) actually follows a Chi-squared distribution. By using all the above equations and integrating over θ, one has

$$P_o = 1 - e^{-\frac{r\left(|K_1|^2+|K_2|^2\right)\left(I+\sigma_Z{}^2\right)}{P_s\sigma_h{}^2}}I_0\left(\frac{2rI|K_1K_2^*|}{P_s\sigma_h^2}\right). \tag{34}$$

4.2 | Symbol error rate

Assuming the signal constellation has M symbols in total, the symbol correct probability of the detector in (17) is:

$$P_r = \frac{1}{M}\sum_{l=1}^{M}P\left[k_l^2 < k_n^2, \forall n \neq l \mid X = x_l\right], \tag{35}$$

where the condition $k_l^2 < k_n^2$ is equivalent to $a_r^2A_l^2 + B_l^2 + 2(a_r\sin\phi_r)A_lB_l < a_r^2A_n^2 + B_n^2 + 2(a_r\sin\phi_r)A_nB_n$. Denote $S_i = S|_{X=x_i}$, $S_{ln}^1 = \mathrm{Re}\{S_l - S_n\}$ and $S_{ln}^2 = \mathrm{Im}\{S_l - S_n\}$. One has $S_{nl}^1 = -S_{ln}^1$, $S_{nl}^2 = -S_{ln}^2$ and $S_{nl} = S_n - S_l$. Thus, $A_n = A_l + S_{ln}^1$, $B_n = B_l + S_{ln}^2$ and

$$\begin{aligned}k_n^2 = &\,a_r^2A_l^2 + B_l^2 + 2(a_r\sin\phi_r)A_lB_l\\ &+ \left(a_r^2S_{ln}^1 + (a_r\sin\phi_r)S_{ln}^2\right)\left(2A_l + S_{ln}^1\right)\\ &+ \left(S_{ln}^2 + (a_r\sin\phi_r)S_{ln}^1\right)\left(2B_l + S_{ln}^2\right).\end{aligned} \tag{36}$$

Denote $V_{nl} = 2A_l - S_{nl}^1 + (2B_l - S_{nl}^2)i = 2(A_l + B_li) - S_{nl}$ and $T_{nl} = a_r^2S_{nl}^1 + (a_r\sin\phi_r)S_{nl}^2 - (S_{nl}^2 + (a_r\sin\phi_r)S_{nl}^1)i$. When $X = x_l$, $V_{nl} = 2N - S_{nl}$ and the inequality $k_l^2 < k_n^2$ is further simplified to $\mathrm{Re}\{NT_{nl}\} < \frac{\mathrm{Re}\{S_{nl}T_{nl}\}}{2}$, where $N = K_1Z + K_2Z^*$ and $\mathrm{Re}\{NT_{nl}\} = \mathrm{Re}\{(K_1T_{nl} + K_2^*T_{nl}^*)Z\}$. Let $c_{nl} = K_1T_{nl} + K_2^*T_{nl}^* = |c_{nl}|e^{j\theta_{c_{nl}}}$. One has $\mathrm{Re}\{(K_1T_{nl} + K_2^*T_{nl}^*)Z\} = |c_{nl}|\,\mathrm{Re}\{Ze^{j\theta_{c_{nl}}}\}$. Because Z is circularly symmetric, $Ze^{j\theta_{c_{nl}}}$ has the same distribution as Z. Thus,

$$P[k_l^2 < k_n^2 \mid X = x_l] \Rightarrow P[\mathrm{Re}\{Z\} < \frac{\mathrm{Re}\{S_{nl}T_{nl}\}}{2|c_{nl}|}]. \tag{37}$$

Since $\mathrm{Re}\{Z\} \sim N(0, \frac{\sigma_Z^2}{2})$, one has

$$\begin{aligned}&\frac{1}{M}\sum_{l=1}^{M}P\left[k_l^2 < k_n^2, \forall n \neq l \mid X = x_l\right]\\ &= \frac{1}{M}\sum_{l=1}^{M}P\left[\mathrm{Re}\{Z\} < \min_{n\neq l}\frac{\mathrm{Re}\{S_{nl}T_{nl}\}}{2|c_{nl}|} \mid X = x_l\right]\\ &= 1 - \frac{1}{M}\sum_{l=1}^{M}Q\left(\min_{n\neq l}\frac{\mathrm{Re}\{S_{nl}T_{nl}\}}{\sqrt{2}|c_{nl}|\sigma_Z}\right).\end{aligned} \tag{38}$$

Therefore, the analytical symbol error rate is

$$P_e = \frac{1}{M}\sum_{l=1}^{M}Q\left(\min_{n\neq l}\frac{\mathrm{Re}\{S_{nl}T_{nl}\}}{\sqrt{2}|c_{nl}|\sigma_Z}\right). \tag{39}$$

By putting the IQI mismatch parameters into (39), one can further has

$$P_e = \frac{1}{M}\sum_{l=1}^{M}Q\left(\min_{n\neq l}\frac{\sqrt{a_r^2(S_{nl}^1)^2 + (S_{nl}^2)^2 + 2(a_r\sin\phi_r)S_{nl}^1S_{nl}^2}}{\sqrt{2}(a_r|\cos\phi_r|)\sigma_Z}\right). \tag{40}$$

5 | NUMERICAL RESULTS AND DISCUSSION

In the numerical results, we set $\sigma_h^2 = \sigma_Z^2 = \sigma_X^2 = 1$. Define $\frac{P_S}{\sigma_Z^2}$ as the average signal-to-noise ratio (ASNR) and $\frac{I}{\sigma_Z^2}$ as the interference-to-noise ratio (INR). We first explore the symmetric IQI case where $a_t = a_r = a$ and $\phi_t = \phi_r = \phi$. All

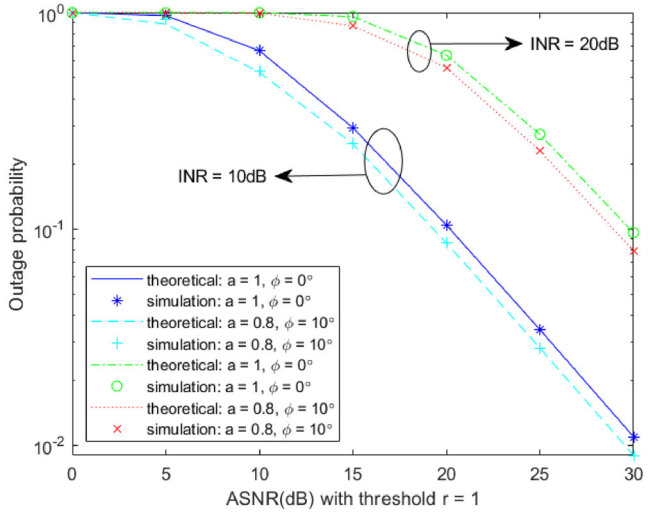

FIGURE 1 Outage probability comparison with $r = 1$

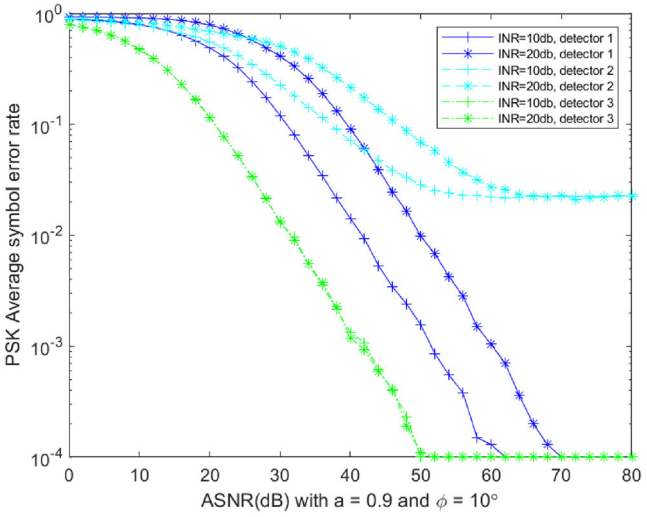

FIGURE 2 SER comparison under perfect CSI

experiments are carried out with 16-PSK modulation scheme. We compare the outage results under different INR level and HWI coefficients. In Figure 1, we set $r = 1$. The curves represent various cases including zero HWI with $(a, \phi) = (1.0, 0°)$, high HWI with $(a, \phi) = (0.8, 10°)$, low INR with INR = 10dB and high INR with INR = 20dB. The simulation matches well with the calculation from (34). It is noted that the outage probability increases with INR but decreases with ASNR. This figure indicates that our derived outage probability is accurate.

Next, we will show the SER performance. We will compare three detectors: detector 1 (noncoherent detector in (26)), detector 2 (noncoherent detector ignoring HWI in (27)) and detector 3 (coherent detector in (17)). Detector 2 is the conventional spectrum sharing detector which does not consider HWI. Thus, it could be used as a SER benchmark. For convenience, we approximate the second term in (26) with $\frac{2\sqrt{I}k_1}{\sigma_Z^2}$. We first set the HWI coefficients to $a = 0.9$ and $\phi = 10°$. In Figure 2, we assume perfect CSI where all relevant parameters that are utilized in each detector are known. We find that the coherent detector is the optimal detector. The result shows that SER of detector 1 is lower than that of detector 2, indicating the necessity of considering HWI. For each detector, increasing ASNR can greatly reduce the SER. Also, note that the performance gain of detector 3 increases as the INR increases. This is because a large radar interference impairs the performances of detector 1 and 2 but detector 3 is robust to it. The result is also consistent with (40). All detectors are found to have a SER floor due to HWI, which is consistent with [17] and [31].

Figure 2 is for perfect CSI. We explore the effect of CSI by using the estimated parameters of h and $\sqrt{I}e^{j\theta}$ with estimation errors as Gaussian $CN(0, \sigma_e^2)$, where σ_e determines the error variance. Figure 3 and Figure 4 display the effects of CSI on the performances of the proposed detectors. Similar to Figure 2, all detectors have an error floor. The overall performance is much degraded compared with the perfect CSI case in Figure 2

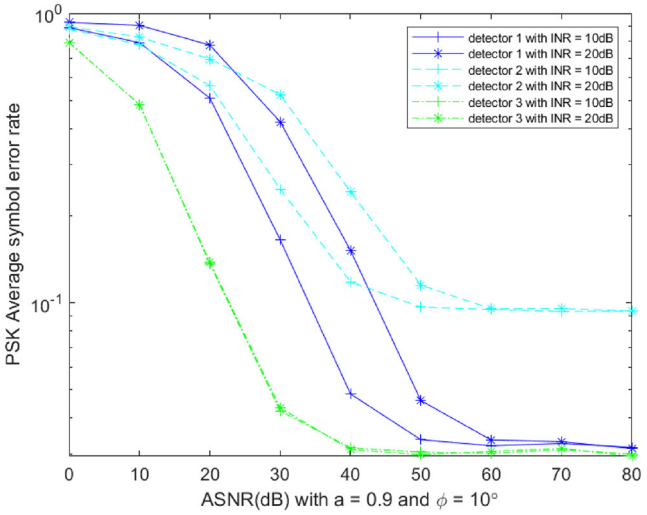

FIGURE 3 SER comparison under CSI of $\sigma_e = 0.05$

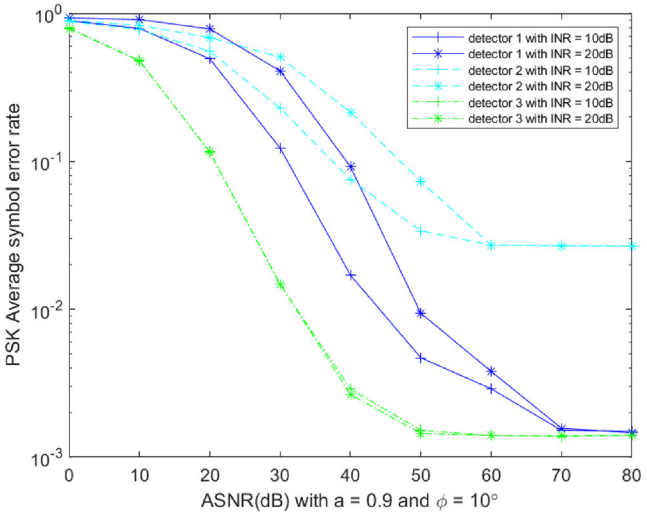

FIGURE 4 SER comparison under CSI of $\sigma_e = 0.01$

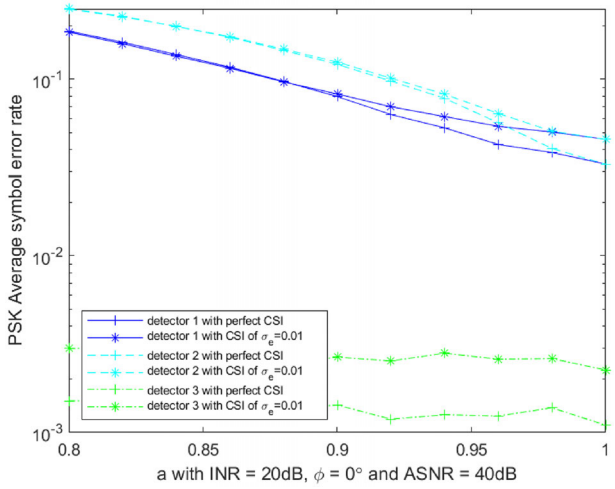

FIGURE 5 The effect of amplitude mismatch a and σ_e

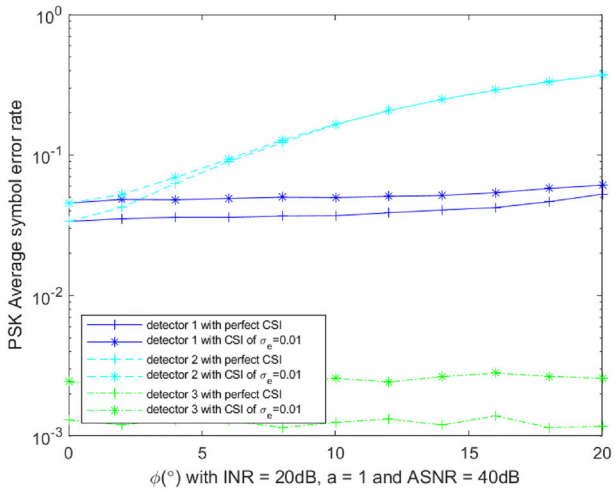

FIGURE 6 The effect of phase mismatch ϕ and σ_e

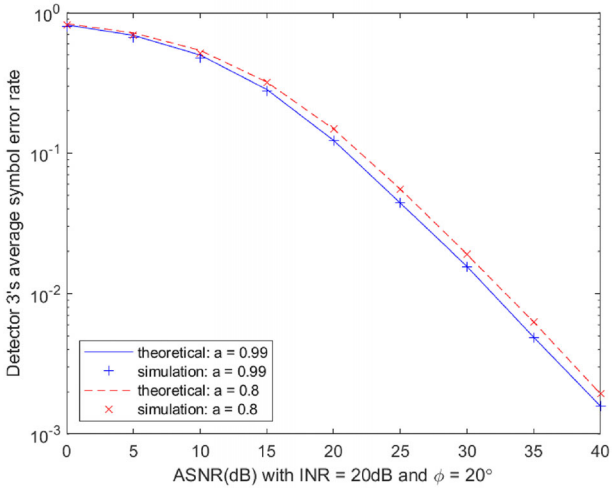

FIGURE 7 The match of theoretical results and simulation results

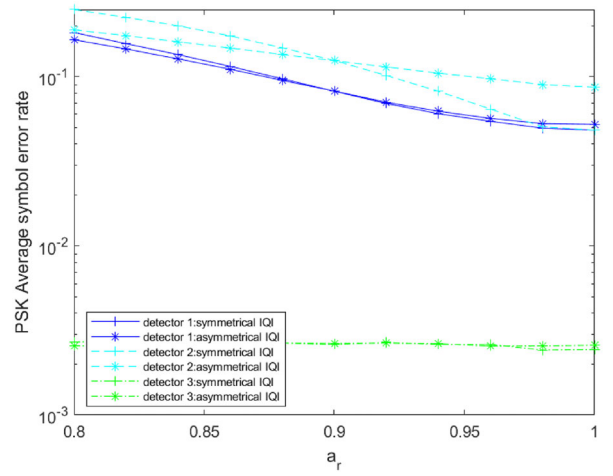

FIGURE 8 The asymmetric case with $a_t = 0.9$, $\phi_t = \phi_r = 0°$, ASNR = 40 dB, INR = 20 dB and $\sigma_e = 0.01$

and smaller σ_e yields better SER performance because it represents the more accurate estimation of the relevant parameters. Different from Figure 2, the performance of the proposed noncoherent detector is quite close to that of the coherent detector at high ASNR. Detector 2 is still the worst and larger radar interference power will further degrade the performance except the proposed coherent detector. Also, note that imperfect CSI will greatly raise the error floor of all detectors.

As the previous figures show, the performance always improves as ASNR gets larger before it reaches the floor. Therefore, we fix ASNR, INR and σ_e to be 40 dB, 20 dB and 0.01, respectively, to investigate the effect of IQI coefficients. In Figure 5, we set ϕ to be zero to explore the effect of a. The coherent detector is found to be robust to a while the other two detectors suffered a lot from a. In this case, σ_e makes no difference when a is small between detector 1 and detector 2. In Figure 6, we explore the effect of ϕ by setting a to be 1. Both the coherent detector and noncoherent detector are not sensitive to ϕ while the noncoherent detector ignoring HWI still suffers a lot from the distortion. This further demonstrates the necessity and value of considering HWI. Another interesting finding is that σ_e gradually turns into making no difference as ϕ increases for detector 2. Figure 7 shows that the simulated SER of detector 3 matches well with theoretical values where INR = 20 dB and $\phi = 20\circ$ with $a \in \{0.99, 0.8\}$. Finally, we explore the impact of IQI amplitude impact in asymmetric case where a_t is fixed to 0.9 and $\phi_t = \phi_r = 0°$ while a_r changes. ASNR, INR and σ_e are set the same as those in Figure 5. In Figure 8, one sees similar results to Figure 5. When a_r exceeds 0.9, the symmetric system outperforms the asymmetric system.

6 | CONCLUSION

In this work, we have considered both radar signal interference and hardware impairment in a joint radar-communications system to investigate its performance in terms of outage probability and symbol error rate. The system is influenced by the

complicated effects of radar interference power, IQI coefficients and CSI. HWI has been shown to be indispensable to evaluate the performance. Radar interference power has been found to significantly influence the noncoherent detectors.

CONFLICT OF INTEREST

The authors declare no conflict of interest.

DATA AVAILABILITY STATEMENT

Data sharing not applicable to this article as no datasets were generated or analysed during the current study.

ORCID

Junqiu Wang https://orcid.org/0000-0001-7120-7381

REFERENCES

1. Sodagari, S., Khawar, A., Clancy, T.C., McGwier, R.: A projection based approach for radar and telecommunication systems coexistence. In: 2012 IEEE Global Communications Conference (GLOBECOM), pp. 5010–5014. IEEE, Piscataway (2012)
2. Saruthirathanaworakun, R., Peha, J.M., Correia, L.M.: Opportunistic sharing between rotating radar and cellular. IEEE J. Sel. Areas Commun. 30(10), 1900–1910 (2012)
3. Khawar, A., Abdelhadi, A., Clancy, T.C.: A mathematical analysis of cellular interference on the performance of s-band military radar systems. In: 2014 Wireless Telecommunications Symposium, pp. 1–8. IEEE, Piscataway (2014)
4. Romero, R.A., Shepherd, K.D.: Friendly spectrally shaped radar waveform with legacy communication systems for shared access and spectrum management. IEEE Access 3, 1541–1554 (2015)
5. Kilani, M.B., Gagnon, G., Gagnon, F.: Multistatic radar placement optimization for cooperative radar-communication systems. IEEE Commun. Lett. 22(8), 1576–1579 (2018)
6. Zheng, H., Li, Y., Zhu, Y.: The communication solution for lte system under radar interference circumstance. Int. J. Antennas Propag. 2015, 849695 (2015)
7. Safavi Naeini, H.A., Ghosh, C., Visotsky, E., Ratasuk, R., Roy, S.: Impact and mitigation of narrow-band radar interference in down-link lte. In: IEEE International Conference on Communications (ICC) 2015, pp. 2644–2649. IEEE, Piscataway (2015)
8. Nartasilpa, N., Salim, A., Tuninetti, D., Devroye, N.: Communications system performance and design in the presence of radar interference. IEEE Trans. Commun. 66(9), 4170–4185 (2018)
9. Zhang, J.A., Rahman, M.L., Wu, K., Huang, X., Guo, Y.J., Chen, S., Yuan, J.: Enabling joint communication and radar sensing in mobile networks–a survey. IEEE Commun. Surv. Tutor. 24(1), 306–345 (2021)
10. Liu, F., Masouros, C., Petropulu, A.P., Griffiths, H., Hanzo, L.: Joint radar and communication design: Applications, state-of-the-art, and the road ahead. IEEE Trans. Commun. 68(6), 3834–3862 (2020)
11. Geng, Z., Xu, R., Deng, H., Himed, B.: Fusion of radar sensing and wireless communications by embedding communication signals into the radar transmit waveform. IET Radar Sonar Navig. 12(6), 632–640 (2018)
12. Liu, X., Huang, T., Shlezinger, N., Liu, Y., Zhou, J., Eldar, Y.C.: Joint transmit beamforming for multiuser mimo communications and mimo radar. IEEE Trans. Signal Process. 68, 3929–3944 (2020)
13. Kumari, P., Choi, J., González.Prelcic, N., Heath, R.W.: Ieee 802.11 ad-based radar: An approach to joint vehicular communication-radar system. IEEE Trans. Veh. Technol. 67(4), 3012–3027 (2017)
14. Barneto, C.B., Riihonen, T., Turunen, M., Anttila, L., Fleischer, M., Stadius, K., Ryynänen, J., Valkama, M.: Full-duplex ofdm radar with lte and 5g nr waveforms: Challenges, solutions, and measurements. IEEE Trans. Microwave Theory Tech. 67(10), 4042–4054 (2019)
15. Dokhanchi, S.H., Mysore, B.S., Mishra, K.V., Ottersten, B.: A mmwave automotive joint radar-communications system. IEEE Trans. Aerosp. Electron. Syst. 55(3), 1241–1260 (2019)
16. Liu, F., Masouros, C., Li, A., Sun, H., Hanzo, L.: Mu-mimo communications with mimo radar: From co-existence to joint transmission. IEEE Trans. Wireless Commun. 17(4), 2755–2770 (2018)
17. Javed, S., Amin, O., Ikki, S.S., Alouini, M.S.: Asymmetric modulation for hardware impaired systems–error probability analysis and receiver design. IEEE Trans. Wireless Commun. 18(3), 1723–1738 (2019)
18. Buzzi, S., Chih.Lin, I., Klein, T.E., Poor, H.V., Yang, C., Zappone, A.: A survey of energy-efficient techniques for 5g networks and challenges ahead. IEEE J. Sel. Areas Commun. 34(4), 697–709 (2016)
19. Costa, E., Pupolin, S.: M-qam-ofdm system performance in the presence of a nonlinear amplifier and phase noise. IEEE Trans. Commun. 50(3), 462–472 (2002)
20. Studer, C., Wenk, M., Burg, A.: Mimo transmission with residual transmit-rf impairments. In: International ITG Workshop on Smart Antennas (WSA) 2010, pp. 189–196. IEEE, Piscataway (2010)
21. Schenk, T.: RF Imperfections in High-Rate Wireless Systems: Impact and Digital Compensation. Springer Science & Business Media, Dordrecht (2008)
22. Inserra, D., Tonello, A.M.: Doa estimation with compensation of hardware impairments. In: IEEE 72nd Vehicular Technology Conference-Fall 2010, pp. 1–5. IEEE, Piscataway (2010)
23. Boulogeorgos, A.A.A., Chatzidiamantis, N.D., Karagiannidis, G.K.: Energy detection spectrum sensing under rf imperfections. IEEE Trans. Commun. 64(7), 2754–2766 (2016)
24. Ding, F., Wang, H., Zhang, S., Dai, M.: Impact of residual hardware impairments on non-orthogonal multiple access based amplify-and-forward relaying networks. IEEE Access 6, 15117–15131 (2018)
25. Balti, E., Guizani, M., Hamdaoui, B., Khalfi, B.: Aggregate hardware impairments over mixed rf/fso relaying systems with outdated csi. IEEE Trans. Commun. 66(3), 1110–1123 (2017)
26. Gao, Y., Chen, Y., Chen, N., Zhang, J.: Performance analysis of dual-hop relaying with i/q imbalance and additive hardware impairment. IEEE Trans. Veh. Technol. 69(4), 4580–4584 (2020)
27. Mokhtar, M., Gomaa, A., Al.Dhahir, N.: Ofdm af relaying under i/q imbalance: Performance analysis and baseband compensation. IEEE Trans. Commun. 61(4), 1304–1313 (2013)
28. Li, J., Matthaiou, M., Svensson, T.: I/q imbalance in af dual-hop relaying: Performance analysis in nakagami-m fading. IEEE Trans. Commun. 62(3), 836–847 (2014)
29. Salim, A., Tuninetti, D., Devroye, N., Erricolo, D.: Modeling the interference of pulsed radar signals in ofdm-based communications systems. In: 2017 IEEE Radar Conference (RadarConf), pp. 0657–0662. IEEE, Piscataway (2017)
30. Chen, Y., Yang, Z., Zhang, J., Alouini, M.S.: Further results on detection and channel estimation for hardware impaired signals. IEEE Trans. Commun. 69(11), 7167–7179 (2021)
31. Liu, Z., Lu, G., Ye, Y., Chu, X.: System outage probability of ps-swipt enabled two-way af relaying with hardware impairments. IEEE Trans. Veh. Technol. 69(11), 13532–13545 (2020)

How to cite this article: Wang, J., Chen, Y.: Performance analysis of communications systems with radar interference and hardware impairment. IET Commun. 1–8 (2022).
https://doi.org/10.1049/cmu2.12489